Acoustic Metasurfaces for Personal Acoustic Spaces

Rudra Goel, Advaith Menon, Cesar Morales Xochipiltecatl, Leyla Ulku
PhD mentor: Alan Liu
Faculty Advisor: Dr. Karthikeyan Sundaresan

***Abstract*—Acoustic metasurfaces are a burgeoning area of interest in the field of acoustic signal processing, thanks to their degree of wavefront manipulation not found in nature. While promising in many applications, especially thanks to their promise in beamforming, little research has been done to implement acoustic metasurfaces to create personal acoustic spaces. This is thanks in part to the difficulty of implementing metasurfaces capable of beamforming a wider band of lower frequencies in the acoustic range. To resolve this issue, we present two labyrinthine metasurfaces exhibiting a near linear phase response characteristic specifically designed for the creation of personal acoustic spaces.**

***Index Terms*—Personal acoustic space, acoustic metasurfaces, metamaterials, passive phased array, wavefront manipulation, beamforming**

I. Introduction

A. Motivation

THIS research aims to harness acoustic metasurfaces in the creation of personal acoustic spaces (PAS). A PAS is an area in which only the desired signal is heard; outside of the space, the desired signal can be completely different [1]. To achieve this, acoustic energy can be steered in such a way that the majority of its energy targets one region and, consequently, areas adjacent to the personal acoustic space experience a reduced level of its noise [2]–[4]. One use case

Fig. 1: Concept of Personal Acoustic Spaces. The green region is where an acoustic signal is directed while the red region becomes a muted zone

of personal acoustic spaces can be imagined in the context of a movie screening in a cinema hall with two different languages simultaneously being played but towards opposing sides of the crowd; the acoustic signal for each language is propagated from the same area yet reaches differing ends and serves two audiences at once. Traditionally, PAS like these have been created by way of acoustic beamforming using speaker arrays. However, to achieve this, an electronically controlled phased array is needed, meaning that a high-speed and high-resolution digital signal processing unit must be present on the system itself in order to produce a phase delay for each speaker accurately. This approach, although robust, increases the cost considerably and is not practical to implement in most cases.

To solve this issue, acoustic metasurfaces can be designed to simulate the beamforming effects of a speaker array [4], [5], each cell acting as a single speaker in the array. This solution significantly reduces cost thanks to removing the need for costly processing units, as well as reducing the necessary number of speakers to one. Not only this, but metasurfaces provide the additional advantage of being highly reconfigurable in the sense that they can be designed to perform any acoustic task a user may require.

Within this paper, we propose a design for a wideband, acoustic metasurface operating in the frequency band 1 - 4 kHz capable of beamforming at angles of 15 and 30 degrees to create personal acoustic spaces. A modular solution is also proposed, layering different combinations of metasurfaces to achieve more extreme results.

Given that a personal acoustic space is dependent on where the user desires most of the acoustic energy to be focused, our approach of 3D printed metamaterial bricks for acoustic beamforming empowers the user to reconfigure the orientation of these blocks and channel acoustic waves in different directions without having to move the speaker source. In effect, personal acoustic spaces themselves become reconfigurable due to the modularity of these metamaterial bricks.

II. Background

Acoustic metamaterials have been of much interest as of late due to their wave-altering properties not found in nature. The force behind these properties are their periodic structures, which may affect resonance or time delay of an incident wave [6]. In considering metasurfaces for practical applications, type, design, properties, and bandwidth must be taken into account.

Regarding wavefront manipulation, two types of metasurface structures are typically considered [7] due to their simple and easily-reconfigurable designs. The first are (i) locally resonant structures, created by a periodic array of Helmholtz Resonators along a straight pipe [2], [5], [8]. The complex impedances created by higher order modes of the

resonators are what give the structure are what give the structure transmission characteristics as described by Li, *et al* [9]. The second are (ii) labyrinthine structures where its geometry is manipulated by bars of varying length and width, spaced evenly on both edges of an empty channel [10]–[12] . The labyrinthine structure is chosen for this study because of its scalability along the azimuthal direction and low impedance.

Existing work in the field of acoustic beamforming via metamaterials has been performed to a great extent [4], [5], [13]. This is demonstrated in He et al's work in constructing a configurable Helmholtz type metasurface that has beamforming capabilities [14]. Each unit in the array is composed of a 2 cell Helmholtz resonator structure with varying depths to allow for phase shifting; this system is backed by a solenoid valve allowing for the depth of each Helmholtz resonator cell to be adjusted and for the bandwidth of the array to extend from 16 kHz to 24 kHz. Although the metamaterial brick allowed for wide-band signals to be beamformed, it required a meticulous setup with electronically controlled solenoid valves adjusting the outgoing angle. With the labyrinthine-based metamaterial, users can adjust the angle of the acoustic waves by simply stacking it in front of a speaker to form a cascade.

A major challenge of using acoustic metasurfaces is the limitations from having a material designed to phase shift a singular frequency; outside of this frequency, the metasurface performs less optimally. Some wideband implementations have been proposed, like CW-AcousLen, which are capable of functioning on a wider band (16-24 kHz specifically for CW-AcousLen) [14]. However, as of yet, there has been little work done to develop a metasurface in the lower frequencies of the acoustic range due to the larger wavelengths; only work focusing on reflecting [15], [16] or absorbing [17], [18] lower frequencies has been done.

The most prevalent gaps throughout research on acoustic metasurfaces and acoustic spaces lie in expanding usable bandwidth of a metasurface, implementing metasurfaces for large-scale use, and using a single metasurface to phase shift many signal types in the desired way. To approach solving these problem gaps, we strive to develop a modular acoustic metasurface with beamforming capability which is the basis for a personal acoustic space. Solving this problem is important because the practical applications of metasurfaces (and personal acoustic spaces) are extremely promising; however, the leap from theory into everyday practice can only be made once the issues with bandwidth and modularity are resolved.

III. Design

Two time delay based labyrinthine metasurfaces were designed due to their ability to maintain a near linear phase response over select frequencies. The structures are symmetric in each horizontal layer as beam forming is only desired along its azimuth. A 8×8 and 16×16 unit cell surface were created in order to produce a redirected angle of 30 °from an incident plane wave.

A. Labyrinthine linear phase response

A labyrinthine type structure was used over a Helmholtz Resonator type metasurface due to their ability to arrive at a predictable near linear phase response. (see (20))

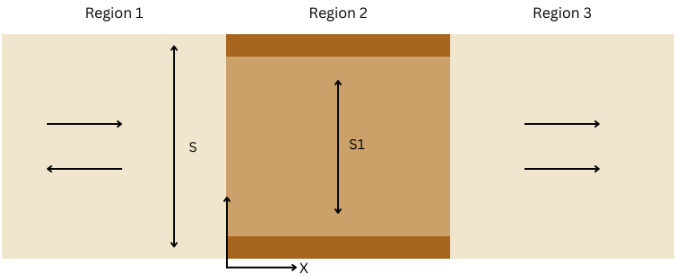

Fig. 2: Incident and transmission boundary region of unit cell

Consider an acoustic plane wave entering the confined channel of a unit cell, with cross-sectional being S and $S1$ respectively (see figure2). The equations of the pressure in each boundary region are as follows:

$$p_1 = A_1 e^{-jkx} + B_1 e^{jkx} \tag{1}$$
$$p_2 = A_2 e^{-jkx} + B_2 e^{jkx} \tag{2}$$
$$p_3 = A_3 e^{-jkx-\ell} \tag{3}$$

And the particle velocity equations respectively being:

$$u_1 = \frac{A_1}{z_0} e^{-jkx} - \frac{B_1}{z_0} e^{jkx} \tag{4}$$
$$u_2 = \frac{A_2}{z_0} e^{-jkx} - \frac{B_2}{z_0} e^{jkx} \tag{5}$$
$$u_3 = \frac{A_3}{z_0} e^{-jk(x-\ell)} \tag{6}$$

With z_0 being the characteristic specific acoustic impedance of air, k being the wave number ($k = \pi/\lambda$), A and B being the propagating coefficients in the $+x$ and $-x$ directions, and ℓ being the channel length. Analyzing the pressure and volume velocity ($U = Su$) boundary conditions between the first and second region ($x = 0$) we see that

$$A_1 + B_1 = A_2 + B_2 \tag{7}$$
$$Su_1 = S_1 u_2 \tag{8}$$
$$S(A_1 - B_1) = S_1(A_2 - B_2) \tag{9}$$

At the boundary between the second and third region ($x = \ell$) we see

$$A_2 e^{-jk\ell} + B_2 e^{-jk\ell} = A_3 \tag{10}$$
$$Su_1 = S_1 u_2 \tag{11}$$
$$S_1(A_2 e^{-jk\ell} - B_2 e^{-jk\ell}) = SA_3 \tag{12}$$

Rewriting the equations, we obtain

$$A_2 = \frac{\left(1 + \frac{S_1}{S}\right) e^{-jk\ell}}{2} A_3 \tag{13}$$
$$B_2 = \frac{\left(1 - \frac{S_1}{S}\right) e^{-jk\ell}}{2} A_3 \tag{14}$$

Writing the previous pair of equations in terms of A_1 and A_3:

$$2A_1 = \left(1 + \frac{S_1}{S}\right) A_2 + \left(1 - \frac{S_1}{S}\right) B_2 \tag{15}$$

$$= \left(\frac{\left(1 + \frac{S_1}{S}\right)\left(1 + \frac{S}{S_1}\right) e^{jk\ell}}{2} \right. \tag{16}$$

$$\left. + \frac{\left(1 - \frac{S_1}{S}\right)\left(1 - \frac{S}{S_1}\right) e^{-jk\ell}}{2} \right) A_3$$

$$= A_3 \left(2\cos k\ell + j\left(\frac{S}{S_1} + \frac{S_1}{S}\sin k\ell\right)\right) \tag{17}$$

With the transmission coefficient defined as $\tau = A_3/A_1$, it can be written as

$$\tau = \frac{2}{2\cos k\ell + j\left(\frac{S}{S_1} + \frac{S_1}{S}\right)\sin k\ell} \tag{18}$$

Taking the argument of the transmission coefficient the phase response of the unit cell is given.

$$\varphi = -\arctan\left(\frac{\left(\frac{S}{S_1} + \frac{S_1}{S}\right)}{2}\frac{\sin k\ell}{\cos k\ell}\right) \tag{19}$$

The effect of the cross-sectional area of S and S_1 can be seen. When the cross-sectional area is comparable $S_1 \approx S$ the phase response simplifies to a basic linear relationship of

$$\varphi = k\ell \tag{20}$$

Here, the phase response of the unit cell is solely a function of the length of the channel and the wave number. To maintain this linear relationship, the channel widths within the labyrinth structure are kept constant throughout.

B. Unit Cell beam forming

To produce a 30° beam from an incident plane wave with the metasurface, each unit cell of the metasurface can be viewed as an isotropic antenna. Considering the symmetry of the metasurface along every horizontal layer (see figure 3a), it can be analyzed as a linear antenna phase array. The phase shift between two antenna elements is given as

$$\Delta\phi = \frac{2\pi d}{\lambda}\sin\theta \tag{21}$$

With θ being our desired refraction angle and d being the distance between each antenna (i.e the width of the unit cell). This can be rewritten as a function of frequency and element number along the array

$$\phi_n = \frac{2\pi d\sin\theta}{c} \cdot nf \tag{22}$$

Knowing that $\frac{2\pi d\sin\theta}{c}$ is a constant value, this gives the phase necessary for a unit cell given a target frequency and element number.

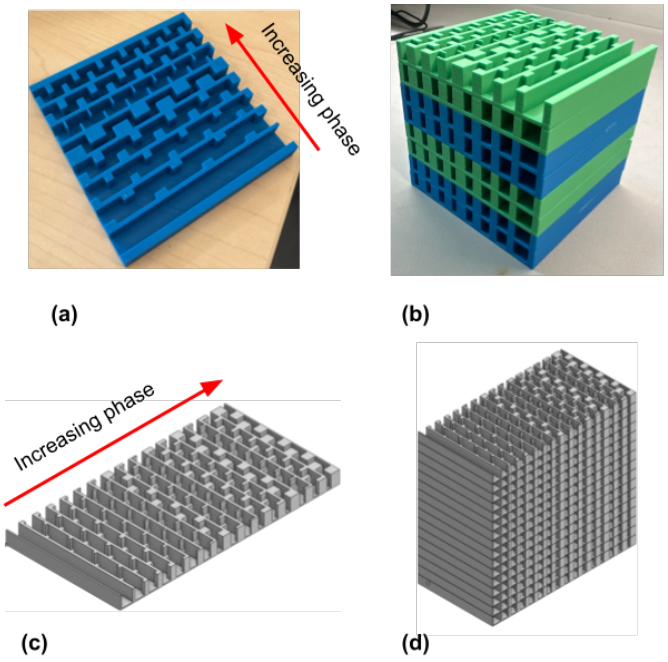

Fig. 3: 8x8 & 16x16 metasurface layers and bricks. (a) and (c) illustrate individual cells increasing in phase as waveguide length increases. (b) & (d) are fully constructed reconfigurable metasurfaces to be placed in front of speakers

C. Labyrinthine Metasurface Design

As mentioned previously with the phased array for beam-forming applications, each unit cell in the metasurface can be thought of as an antenna with a unique time delay; arranging these cells adjacent to each other creates a phased array. Figure 3 demonstrates both in the case of an 8x8 metasurface and 16x16 metasurface that are able to beamform in the azimuth direction.

In order to design a unit cell (or antenna) with a specific phase that sits in the overall phased array, one must consider the geometrical implications of the bar spacing and bar widths that make up the labyrinthine type structure. As mentioned by Liang and Li [19], the coiling-up acoustic metasurface, otherwise known as the labyrinthine type, is a structure that can be characterized by the total length of the waveguide created by the bar structure within. By adding bars of various widths throughout the metasurface channel and and placing them equidistant to one another, the overall length of the waveguide in the cell effectively increases and forces the incident acoustic wave to travel in a zigzag pattern as opposed to a straight line pattern of a plane wave propagating through an open channel, as highlighted by the models in Figure 4. The added distance of the waveguide has a significant impact on the incident wave and produces a time delay to the wave that exits.

2D pressure acoustic simulations performed in COMSOL highlight a phase response of increasing magnitude across a 4kHz bandwidth. By simply adding more bars of equal length and distance from one another, the effective length of the waveguide increases, and consequently, the time delay

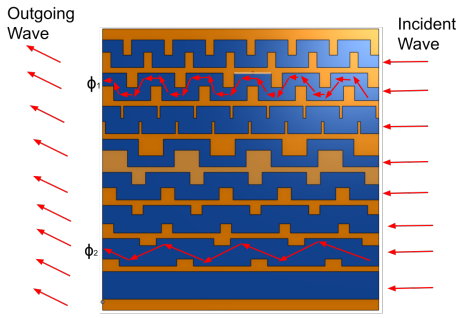

Fig. 4: Individual cells in 8x8 metamaterial. Highlighted in blue is the path of the acoustic wave (waveguide) and is delayed more as the number of bars and its sizing increases. Here $\phi_1 > \phi_2$

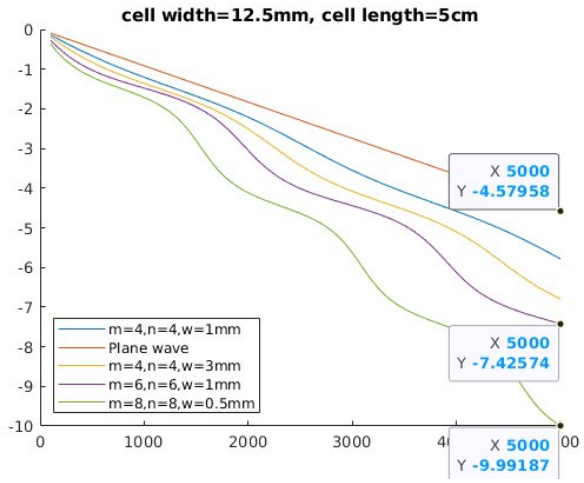

Fig. 5: Phase response for a single unit cell of width 12.5mm and length 5cm.

of the incoming acoustic wave increases as it travels through the metasurface. Figure 5 illustrates how the phase response of structures with increasingly longer waveguides scales in proportion; the length of the waveguide is derivative to the number of top bars m and number of bottom bars n as seen in Figure 4.

However, in order to maintain the linearity condition outlined in equation (20) for the phase response, $S \approx S_1$, the bar lengths and widths are chosen carefully so that the width of the waveguide throughout the coiling space is uniform. When greater phases are desired for a given unit cell, and the difference between S & S_1 is large enough to violate the linearity condition, we simply increase the amount of bars while reducing the length of each the bar to ensure the linear equation (20) can suffice as the phase response as opposed to equation (19). As seen in Figure 5, the phase response increases as the bar width thickens and/or the number of bars on the top (m) and bottom (n) increases.

IV. Evaluation

A. Linearity of designed metasurface

Various values of m (number of upper bars), n (number of lower bars) and w (width of bars) were chosen for the metasurface, and a phase response was generated accordingly (Figure 5).

According to the simulated results, the cell with 4 upper bars, 4 lower bars, and a bar width of 1 mm produced the most linear response, therefore it was with these parameters in mind that a single unit cell could be designed. This single unit cell was then used to create a 16 by 16 cell metasurface in COMSOL. In the simulation, a sound source was placed in a reflective chamber 5 cm away from the metasurface.

In simulating the metasurfaces, the sound pressure level vs. frequency plots shown in Figure 13 were generated for phases -60°to 60°. As demonstrated in the simulations, the 16 by 16 cell metasurface designed to beamform 15 °from center is capable of introducing a considerable phase shift from approximately 1.5 kHz onwards with a gap of approximately 20 dB between -45°and 45°at approximately 2 kHz.

In the 16 by 16 cell metasurface designed to beamform 30 degrees from center, there is a wider gap between simulated

Fig. 6: Pressure vs frequency of 16 by 16 cell, 15 degrees metasurface.

phases thanks to the more extreme angle. As a result, it's shown that sound pressure level for more phases is considerably attenuated. When beamforming at 15 degrees, notably -60 degrees to -30 degrees has significant attenuation to approximately 50 dB from 70 dB at 2.5 kHz and 3 kHz. In contrast with this, the 16 by 16 cell beamforming 30 degrees has significant minima for phases -60 degrees to 0 degrees occurring at 1.8 kHz, 2.5 kHz, and 3.5 kHz.

Through the use of this simulation, it was confirmed that the designed metasurfaces could provide a significant phase delay for frequencies above 1 kHz on a wideband scale. Additionally, it was demonstrated that the two cell types have different beamwidths capable of steering the beam differently at different phases.

B. Implementation

The experimental setup consists of a passive speaker, an amplifier, a plane wave tube for each metasurface, and measurement microphones. The metasurface is placed in the middle of the tube laterally, with all gaps closed using styrofoam to prevent acoustic leakage and isolate the metasurface. Measurements are then taken (i) at various, fixed points around the map (ii) at various angles a fixed radius away from the metasurface. Data is collected using REW at each of these points, with the aid of a frequency sweep starting from 250Hz to 10 kHz. The measurements were taken in a room with minimal furniture to prevent reflective interference.

The metasurface itself is constructed by 3D printing each unit cell using PLA via fuse-deposition modeling (FDM) and then super-gluing each layer together. The dimensions of the metasurfaces are both 192mm x 100mm x 176mm. Both of these metasurfaces beamform either 15 or 30 degrees to the left with respect to the sound source. The plane wave tube for the metasurface is made of acrylic, in the shape of a cuboid and

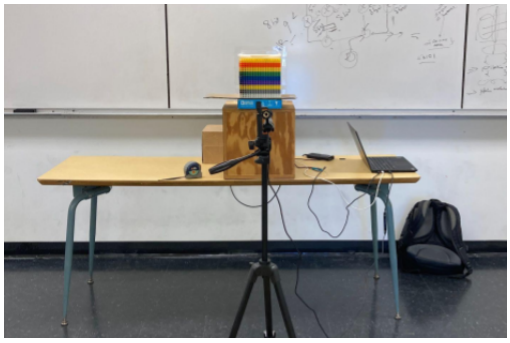

Fig. 7: Experimental setup for 16x16, 30°metasurface.

is of approximate dimensions 195mm x 105 mm x 352 mm. The speaker used for both experiments is 250 watts, located at the center of the back face of both plane wave tubes.

C. Performance metrics

The relative sound pressure level (SPL) is used at each point to determine if the wave was beamformed in the correct direction. Two additional metrics are used: gain at different frequencies, and directionality.

D. Directionality

To measure the directionality of the two metasurfaces, 9 frequency sweeps were simulated then conducted, changing the metasurface's angle to the microphone from -60 to 60 degrees in increments of 5 degrees to confirm that the metasurface was beamforming at the desired angle. The initial simulations were performed in COMSOL to confirm design functionality, then tested both indoors and outdoors to gauge performance differences.

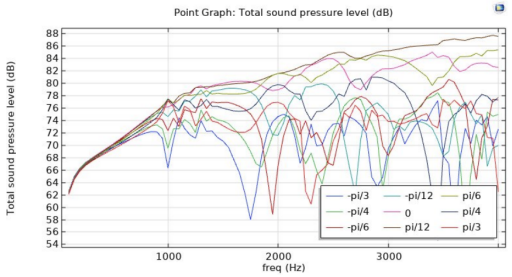

Fig. 8: Pressure vs frequency of 16 by 16 cell, 15 degrees metasurface.

This can be seen thanks to sound pressure being most extreme at 30 degrees; because the frequency sweep was conducted using a 16 by 16, 30 degree metasurface, at 30 degrees, the point of measurement is essentially measuring the beam straight on, thus measuring the most extreme, magnified part of the beam. Similarly, -60 degrees demonstrates the smallest sound pressure level thanks to the same reasoning; the most attenuated part of the beam is being measured at this angle.

Moving to field testing, both indoors and outdoors trials were conducted to measure Sound Pressure Level as a function of angle. These tests were performed 2 meters away from a microphone, turning 5 degrees at a time to capture the full azimuth of the 15 and 30 degree metasurfaces.

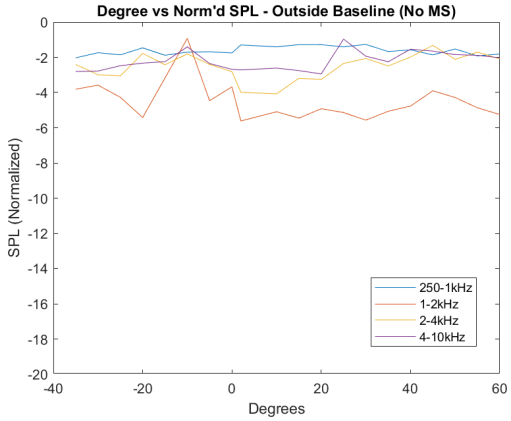

Fig. 9: Pressure vs. Frequency of speaker with no metasurface attached.

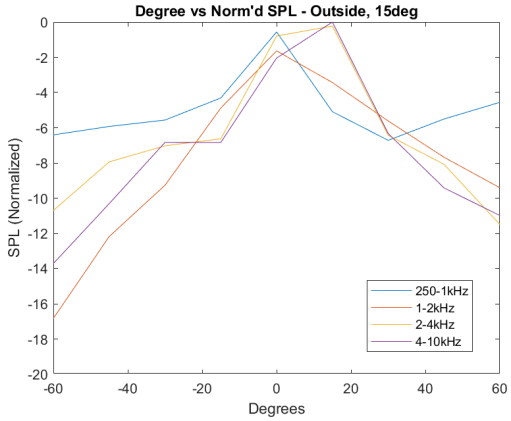

Fig. 10: Pressure vs frequency of 16 by 16 cell, 15 degrees metasurface.

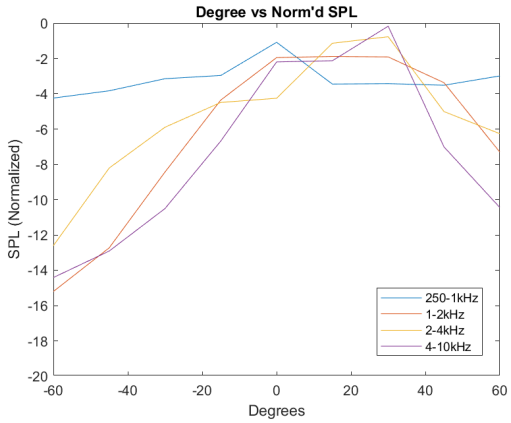

Fig. 11: Pressure vs frequency of 16 by 16 cell, 15 degrees metasurface.

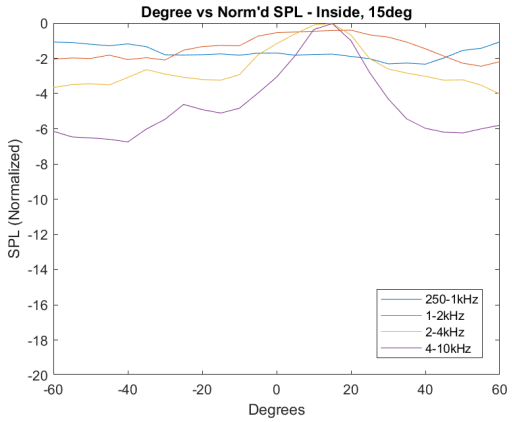

Fig. 12: Pressure vs frequency of 16 by 16 cell, 15 degrees metasurface.

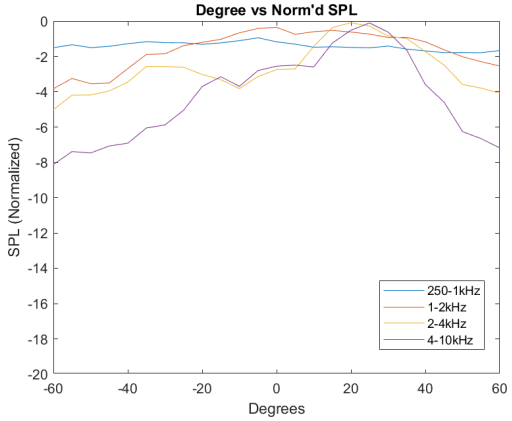

Fig. 13: Pressure vs frequency of 16 by 16 cell, 15 degrees metasurface.

E. Gain

To measure gain, sound pressure was measured on a grid of locations placed around the metasurface.

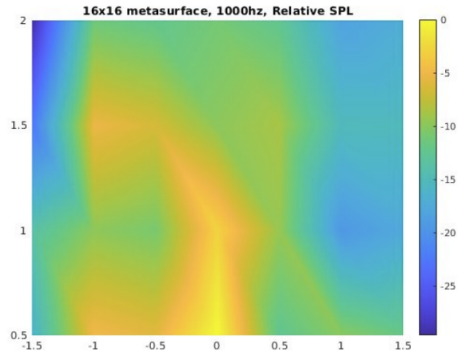

Fig. 14: Gain of 16 by 16 cell metasurface beamforming at 30 degrees.

In Figure 14, it's shown that at (1,0), there is a gain of 0 dB, proving successful beamforming at 30°(in contrast with a gain of approximately -15 dB directly on the right side of x = 0).

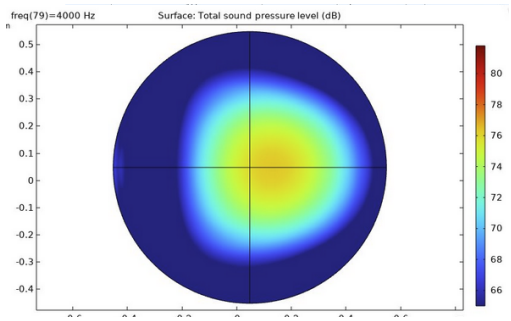

Fig. 15: Heatmap of sound pressure level for cascaded 30 degree 16 by 16 cell metasurface and 15 degree 16 by 16 cell metasurface.

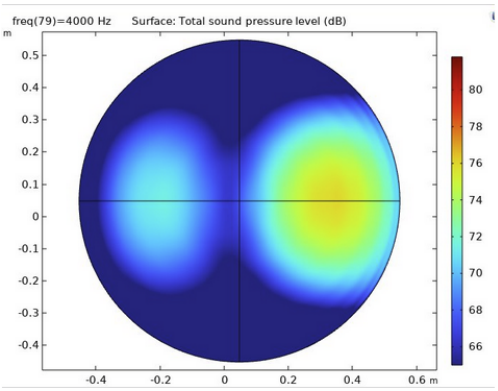

Fig. 16: Heatmap of sound pressure level for cascaded 30 degree 16 by 16 cell metasurface and -15 degree 16 by 16 cell metasurface.

F. Cascaded Metasurfaces

In addition to the measurements taken of the individual metasurface cells, further measurements were simulated in COMSOL of combined 16 by 16 and 16 by 16 metasurfaces with different phase offsets. Each cascaded metasurface is composed of a 16 by 16 cell metasurface closest to the speaker, followed by an 16 by 16 cell metasurface to provide more exaggerated phase differences in different areas of the room.

Two different test cases have been simulated thus far; a 30 degree 16 by 16 cell followed by a 15° 16 by 16 cell or a -15°16 by 16 cell. The former provides less extreme, but slightly more amplified beamforming as shown in Fig 17. The phases are distributed more closely, which is due to the smaller phase difference between the two metasurfaces.

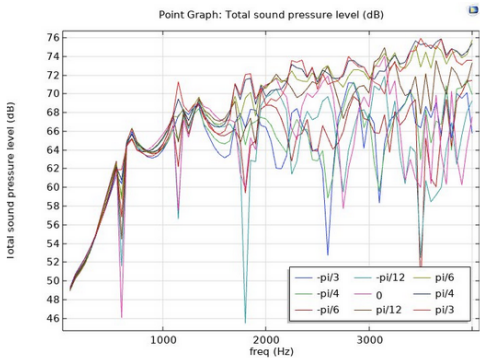

Fig. 17: Staggered metasurface design (30 degrees cascaded with 15 degrees)

REFERENCES

[1] M. Itani, T. Chen, T. Yoshioka, and S. Gollakota, "Creating speech zones with self-distributing acoustic swarms," *Nature Communications*, vol. 14, 1 2023, ISSN: 20411723. DOI: 10.1038/s41467-023-40869-8.

[2] H. Emoto, Y. Noguchi, and T. Yamada, "Acoustic metasurfaces designed via topology optimization for regional sound insulation," *Journal of Sound and Vibration*, vol. 567, 2023, ISSN: 10958568. DOI: 10.1016/j.jsv.2023.117939.

[3] S. A. Cummer, J. Christensen, and A. Alù, *Controlling sound with acoustic metamaterials*, 2016. DOI: 10.1038/natrevmats.2016.1.

[4] P. Chiariotti, M. Martarelli, and P. Castellini, "Acoustic beamforming for noise source localization – reviews, methodology and applications," *Mechanical Systems and Signal Processing*, vol. 120, 2019, ISSN: 10961216. DOI: 10.1016/j.ymssp.2018.09.019.

[5] Z. Chen, S. Shao, M. Negahban, and Z. Li, "Tunable metasurface for acoustic wave redirection, focusing and source illusion," *Journal of Physics D: Applied Physics*, vol. 52, 39 2019, ISSN: 13616463. DOI: 10.1088/1361-6463/ab2abd.

[6] B. Assouar, B. Liang, Y. Wu, Y. Li, J.-C. Cheng, and Y. Jing, "Acoustic metasurfaces," *Nature Reviews Materials*, vol. 3, pp. 460–472, Dec. 2018, ISSN: 2058-8437. DOI: 10.1038/s41578-018-0061-4. eprint: https://www.nature.com/articles/s41578-018-0061-4.pdf. [Online]. Available: https://doi.org/10.1038/s41578-018-0061-4.

[7] J. Guo, Y. Fang, R. Qu, and X. Zhang, "Development and progress in acoustic phase-gradient metamaterials for wavefront modulation," *Materials Today*, vol. 66, pp. 321–338, 2023, ISSN: 1369-7021. DOI: https://doi.org/10.1016/j.mattod.2023.04.004. [Online]. Available: https://www.sciencedirect.com/science/article/pii/S1369702123001086.

[8] L. Ye, C. Qiu, J. Lu, *et al.*, "Making sound vortices by metasurfaces," *AIP Advances*, vol. 6, 8 2016, ISSN: 21583226. DOI: 10.1063/1.4961062.

[9] Y. Li, S. Qi, and M. B. Assouar, "Theory of metascreen-based acoustic passive phased array," *New Journal of Physics*, vol. 18, no. 4, p. 043 024, 2016. DOI: 10.1088/1367-2630/18/4/043024. [Online]. Available: https://dx.doi.org/10.1088/1367-2630/18/4/043024.

[10] G. Memoli, M. Caleap, M. Asakawa, D. R. Sahoo, B. W. Drinkwater, and S. Subramanian, "Metamaterial bricks and quantization of meta-surfaces," *Nature Communications*, vol. 8, 2017, ISSN: 20411723. DOI: 10.1038/ncomms14608.

[11] A. Azbaid El Ouahabi and G. Memoli, "A transfer matrix method for calculating the transmission and reflection coefficient of labyrinthine metamaterials," *The Journal of the Acoustical Society of America*, vol. 151, no. 2, pp. 1022–1032, Feb. 2022, ISSN: 0001-4966. DOI: 10.1121/10.0009428. eprint: https://pubs.aip.org/asa/jasa/article-pdf/151/2/1022/16522215/1022_1_online.pdf. [Online]. Available: https://doi.org/10.1121/10.0009428.

[12] J. Chen, J. Xie, and J. Liu, "Continuous-phase-transformation acoustic metasurface," *Results in Physics*, vol. 30, 2021, ISSN: 22113797. DOI: 10.1016/j.rinp.2021.104840.

[13] D. Yun, T. R. Jennings, G. Kidd, and M. J. Goupell, "Benefits of triple acoustic beamforming during speech-on-speech masking and sound localization for bilateral cochlear-implant users," *The Journal of the Acoustical Society of America*, vol. 149, 5 2021, ISSN: 0001-4966. DOI: 10.1121/10.0003933.

[14] J. He, J. Xiong, W. Hu, *et al.*, "Cw-acouslen: A configurable wideband acoustic metasurface," in *MOBISYS 2024 - Proceedings of the 2024 22nd Annual International Conference on Mobile Systems, Applications and Services*, Association for Computing Machinery, Inc, Jun. 2024, pp. 29–41, ISBN: 9798400705816. DOI: 10.1145/3643832.3661882.

[15] J. Zhao, B. Li, Z. N. Chen, and C. W. Qiu, "Redirection of sound waves using acoustic metasurface," *Applied Physics Letters*, vol. 103, 15 2013, ISSN: 00036951. DOI: 10.1063/1.4824758.

[16] Y. Cheng, C. Zhou, B. G. Yuan, D. J. Wu, Q. Wei, and X. J. Liu, "Ultra-sparse metasurface for high reflection of low-frequency sound based on artificial mie resonances," *Nature Materials*, vol. 14, 10 2015, ISSN: 14764660. DOI: 10.1038/nmat4393.

[17] J. Ji, D. Li, Y. Li, and Y. Jing, "Low-frequency broadband acoustic metasurface absorbing panels," *Frontiers in Mechanical Engineering*, vol. 6, 2020, ISSN: 22973079. DOI: 10.3389/FMECH.2020.586249.

[18] K. Zeng, Z. Li, Z. Guo, and Z. Wang, "Reconfigurable and phase-engineered acoustic metasurfaces for broadband wavefront manipulation," *Advanced Physics Research*, vol. 3, 4 2024, ISSN: 2751-1200. DOI: 10.1002/apxr.202300128.

[19] Z. Liang and J. Li, "Extreme acoustic metamaterial by coiling up space," *Phys. Rev. Lett.*, vol. 108, p. 114 301, 11 2012. DOI: 10.1103/PhysRevLett.108.114301.

[Online]. Available: https://link.aps.org/doi/10.1103/PhysRevLett.108.114301.